

Fano resonances in tilted Weyl semimetals in an oscillating quantum well

Souvik Das^{♣,1}, Arnab Maity^{♣,1}, Rajib Sarkar^{♣,1}, Anirudha Menon,² Tanay Nag,^{3,4} and Banasri Basu⁵

¹Indian Institute of Science, Education, and Research, Kolkata, India

²School of Physical Sciences, Indian Association for the Cultivation of Sciences, Kolkata, India

³Department of Physics, BITS Pilani-Hyderabad Campus, Telangana 500078, India

⁴Department of Physics and Astronomy, Uppsala University, Box 516, 75120 Uppsala, Sweden

⁵Physics and Mathematics Unit & Interdisciplinary Statistical Research Unit, Indian Statistical Institute, Kolkata, India*

(Dated: August 1, 2023)

Considering low-energy model of tilted Weyl semimetal, we study the electronic transmission through a periodically driven quantum well, oriented in the transverse direction with respect to the tilt. We adopt the formalism of Floquet scattering theory and investigate the emergence of Fano resonances as an outcome of matching between the Floquet sidebands and quasi-bound states. The Fano resonance energy changes linearly with the tilt strength suggesting the fact that tilt-mediated part of quasi-bound states energies depends on the above factor. Given a value of momentum parallel (perpendicular) to the tilt, we find that the energy gap between two Fano resonances, appearing for two adjacent values of transverse (collinear) momentum with respect to the tilt direction, is insensitive (sensitive) to the change in the tilt strength. Such a coupled (decoupled) behavior of tilt strength and the collinear (transverse) momentum can be understood from the tilt-mediated and normal parts of the quasi-bound state energies inside the potential well. We vary the other tilt parameters and chirality of the Weyl points to conclusively verify exact form of the tilt-mediated part of the quasi-bound state energy that is the same as the tilt term in the static dispersion. Our work paves the way to probe the tilt-mediated part of quasi-bound state energy for understanding the complex interplay between the tilt and Fano resonance.

I. INTRODUCTION

Weyl semimetals (WSMs) have been the topic of extended research in condensed matter physics over the past decade [1–6], with the proposal for and discovery of the Weyl fermion. This leads to a plethora of theoretical as well as experimental studies focussing on the features, characteristics, and transport properties of such materials [7]. The minimal model of a time reversal symmetry broken WSM consists of two Weyl points which act as a source and sink for Berry curvature in momentum space. These points are usually observed near the Fermi surface where the lightcone like dispersion of the WSM meet [1–4, 8–10]. The first proposed WSMs are now defined in the literature as the type-I WSM, which has a conical dispersion in momentum space. The addition of a Lorentz symmetry violating tilt term to the WSM Hamiltonian gives rise to a new type of WSM called the type-II WSM [11–13]. The type-II phase arises when the value of tilt generally exceeds the Fermi velocity, and this phase has some features which are distinct from the type-I phase including an extended Fermi surface. WSMs irrespective of their types typically exhibit a large variety of exotic properties like negative magneto-resistance [14], universal quantum Hall signatures [3, 15–18], and the chiral magnetic effect [15], all of which are consequences of the chiral anomaly. Importantly, the transport properties of type-II WSMs are starkly different from those of the

type-I phase [19–22]. This can be ascribed to marked differences in the density of states at the Fermi level [11]. Note that type-II WSMs embrace a variant of the chiral anomaly when the magnetic field direction is along the tilt. They possess novel quantum oscillations due to momentum space Klein tunneling [23], and a modified anomalous Hall conductivity [24]. Tilting of the Weyl cones also affects Fano factor as described in [25]. Therefore, one can infer that the tilt-mediated transport phenomena attracted a lot of attention in recent years.

The study of periodically driven systems has always been of great interest to physicists because of the potential to alter material behavior [26–37] and obtain phenomena which may be controlled in a lab environment. Periodic driving is best described by employing the Floquet formalism [38–40], which is the temporal analog of Bloch's theorem in frequency space. The technique utilizes the time periodicity of the driving potential to express the wavefunction as the product of a phase and a periodic function in time, reducing the complexity to solve the time-dependent Schrödinger equation. Advances in Floquet methods have led to the development of Floquet perturbation theory in the form of the high-frequency and van-Vleck expansions [41, 42] where an effective time-independent Floquet Hamiltonian can be obtained. Such methods have been applied to Dirac semimetals [43], WSMs [41, 42], and even quantum spin liquids [44], to generate controllable transport properties. The process of generating tunable band structures in materials is known as functionalizing materials.

In the context of transmission spectra, Fano resonances have been studied in many areas of physics since its inception in 1935 [45]. It is characterized by a perfect

*Electronic address: sribbasu1@gmail.com; ♣SD, AM and RS contributed equally.

transmission followed by a total reflection or vice-versa, leading to an asymmetric resonance profile. The phenomenon can be explained by considering the interaction of localized states with a range of propagating continuum modes, wherein the transmission enhancement occurs due to constructive interference, and the reflection enhancement due to destructive interference, between different quantum trajectories. In the context of non-adiabatically driven quantum systems, Floquet sidebands are formed, and when one of these approaches a quasi-bound state a Fano resonance occurs. Fano resonances have been found to be associated with light propagation in photonic devices [46, 47], scattering in mesoscopic transport systems [46, 48–58] and superconducting Josephson junctions [46, 59], graphene [60], Dirac semimetals [61], and WSMs [62].

A few previous literature dealt with the Fano resonance structure of Dirac [61] and Weyl systems [63] employing Floquet theory in the presence of a harmonically driven potential well. However, there is not much commentary on the consequences of tilt in the energy dispersion on Fano resonances in these cases [64]. Considering the fact that tilt appears to be a key factor in manipulating properties of WSMs as described previously [23–25], and motivated by the importance of transport and Fano resonances, we here examine the role of tilting on Fano resonances in 3D WSMs in this work. In particular we examine the Fano resonances, exploiting the Floquet scattering theory formalism, as a function of tilt strength on type-I and type-II WSMs and uncover hitherto unexplored physics in this context where tilt direction (say along z -axis) is transverse to the transport through the harmonically driven potential well (say along x -axis). Given a value of tilt momentum, we find that the Fano resonance energies depend linearly on the tilt strength while the energy gap between two Fano resonances, appearing for two adjacent values of transverse momentum (say along y -axis) remains insensitive to the change in the tilt strength. On the other hand, given a value of transverse momentum, Fano resonance energies depends linearly on tilt strength and the corresponding tilt momentum in a coupled manner such that the energy gap between two Fano resonances, occurring for two adjacent values of tilt momentum, changes with the variation in the tilt strength. The seclusive (inclusive) behavior between tilt strength and the transverse (collinear) momentum with respect to tilt direction is essentially caused by tilt-mediated and normal parts of the quasi-bound state energies inside the potential well. We also investigate the effect of chirality on the transmission spectra in the above cases to further strengthen the plausible argument. This allows us to understand the interplay between the tilt and Floquet scattering leading to the emergence of Fano resonance through a harmonically driven potential well for 3D WSM.

The structure of this manuscript is as follows: In Sec. II we consider the minimal model of a time reversal symmetry broken WSM with tilt, capable of hosting the type-

I and type-II phases, and introduce the harmonically driven quantum well. Sec. III contains the solution to Schrodinger's equation and formulation of the S-matrix. We present the results for the transmission coefficients in Sec. IV for varying tilts, where the characteristic Fano resonances are demonstrated. A discussion on the results and the implications on future research is presented in Sec. V. We summarize our finding and conclude in Sec. VI.

II. MODEL AND TIME-DEPENDENT QUANTUM WELL

We begin our study by considering the low-energy minimal model around a Weyl point of chirality s as given below [22]

$$H = 2k_z[t_1 \sin(\phi_1 - sk_0) + 2t_2 \sin(\phi_2 - 2sk_0)]\sigma_0 + t(\sigma_x k_x + \sigma_y k_y) + st_z \sigma_z k_z \sin k_0, \quad (1)$$

where $\sigma_x = \begin{pmatrix} 0 & 1 \\ 1 & 0 \end{pmatrix}$, $\sigma_y = \begin{pmatrix} 0 & -i \\ i & 0 \end{pmatrix}$ and $\sigma_z = \begin{pmatrix} 1 & 0 \\ 0 & -1 \end{pmatrix}$ are Pauli matrices. t_z and t are the spatially non-isotropic Fermi velocities of the Weyl nodes. Here the identity term causes a tilt along the k_z direction where $t_{1,2}$ denotes the tilt strength. The phase factors $\phi_{1,2}$ represent the fluxes in hopping along z -direction in a lattice regularized model where the Weyl points appear at $(0, 0, sk_0)$. Note that the tilt term can be finite even when $\phi_{1,2} = 0$ indicating the fact that finite $t_{1,2}$ is essentially responsible for a tilted dispersion. The degree of tilt η_s for a given Weyl point of chirality s is defined as

$$\eta_s = \left| \frac{2[t_1 \sin(\phi_1 - sk_0) + 2t_2 \sin(\phi_2 - 2sk_0)]}{st_z \sin k_0} \right|. \quad (2)$$

This can be evaluated separately for each node to get the type-I ($\eta_s < 1$) and type-II ($\eta_s > 1$) WSM phases in general with $s = \pm 1$. $\eta_s = 1$ marks a Lifshitz phase transition which alters the nature of the Fermi surface as has been observed in the two phases. The dispersion relation, associated with the Hamiltonian, is given by

$$E_{s,u} = 2k_z[t_1 \sin(\phi_1 - sk_0) + 2t_2 \sin(\phi_2 - 2sk_0)] + u\sqrt{t^2(k_x^2 + k_y^2) + t_z^2 k_z^2 \sin^2 k_0}, \quad (3)$$

where $u = \pm$ represent the conduction and valence bands. The Hamiltonian hosts both type-I and type-II phases of a WSM as depicted in Figs. 1 (a-h). The band dispersion $E_{s,u}$ along the tilt momentum k_z for type-I and type-II phases are depicted in Figs. 1 (a,c,e,g) and (b,d,f,h), respectively.

We now choose to subject this system to a harmonically driven quantum well in the x -direction. The potential $V(t)$ for the well is defined as [60, 64, 65],

$$V(t) = \begin{cases} -V_0 + V_1 \cos(\omega t) & -L/2 \leq x \leq L/2 \\ 0 & |x| > L/2 \end{cases} \quad (4)$$

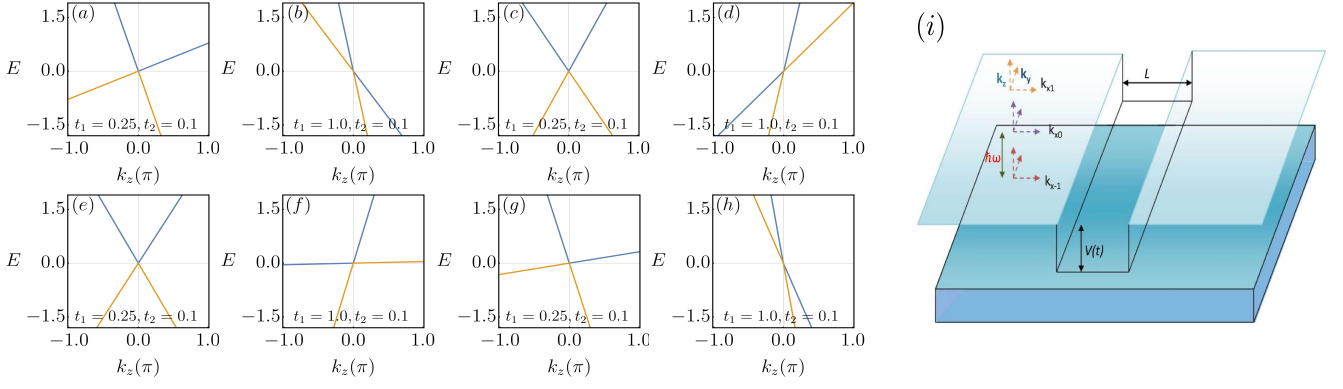


FIG. 1: The dispersion for the Hamiltonian in Eq. (1) are shown in (a-h). We consider $(\phi_1, \phi_2) = (\pi/4, \pi/2)$ and $(\pi, \pi/2)$ in (a,b) and (c,d) [(e,f) and (g,h)], respectively for $s = +1$ [$s = -1$]. The yellow and blue bands represent $E_{s,-}$ and $E_{s,+}$ as given in Eq. (3). We choose $t = t_z = 1$, $k_x = k_y = 0$ and $k_0 = \pi/2$. (i): The potential landscape is shown where the electron is transported in the x -direction through a harmonically driven potential $V(t) = -V_0 + V_1 \cos(\omega t)$ of width L . This potential landscape is only applicable along x -direction which is perpendicular to the direction of tilt. $\hbar\omega$ represents the photon energy for virtual processes, and k_{xi} represent the various momenta for the Floquet sidebands with $i = -1, 0, 1$.

where V_0 is the depth of the static potential well. V_1 and ω denote the amplitude and frequency of the harmonic drive. The setup of our system is shown in Fig. 1 (i), where the qualitative features of the driving potential in the three regions of interest are shown explicitly. The harmonically driven quantum well is confined to a region of width L in the x -direction, while such potential landscape is absent in the z, y -directions. There is no potential outside of this specified region. The electron wavefunctions is simply plane waves along the z, y -directions while x -component is non-trivial. It is very important to note that the tilt and the direction of flow of electrons are in mutually perpendicular as this will have a significant role to play in our results.

III. FLOQUET S-MATRIX

Let us define the wave function as a two component spinor $\psi = \begin{pmatrix} \psi_1 \\ \psi_2 \end{pmatrix}$, and with this, we now solve

$$\psi_n = e^{-iEt/\hbar + ik_y y + ik_z z} \begin{cases} A_n^i N_{n+} \begin{pmatrix} 1 \\ S_+(E_n) \end{pmatrix} e^{ik_{xn}x} + A_n^o N_{n-} \begin{pmatrix} 1 \\ S_-(E_n) \end{pmatrix} e^{-ik_{xn}x}, & x < -L/2 \\ \sum_{m=-\infty}^{\infty} [a_m N'_{m+} \begin{pmatrix} 1 \\ S'_+(E_m) \end{pmatrix} e^{iq_{xm}x} + b_m N'_{m-} \begin{pmatrix} 1 \\ S'_-(E_m) \end{pmatrix} e^{-iq_{xm}x}] J_{n-m} \left(\frac{V_1}{\hbar\omega} \right), & -L/2 \leq x \leq L/2 \\ B_n^i N_{n-} \begin{pmatrix} 1 \\ S_-(E_n) \end{pmatrix} e^{-ik_{xn}x} + B_n^o N_{n+} \begin{pmatrix} 1 \\ S_+(E_n) \end{pmatrix} e^{ik_{xn}x}, & x > L/2 \end{cases} \quad (6)$$

Here $N_{n\pm} = \frac{1}{\sqrt{1+|S_{\pm}(E_n)|^2}}$ and $N'_{m\pm} = \frac{1}{\sqrt{1+|S'_{\pm}(E_m)|^2}}$ are the appropriate normalizing factors, and $A_n^{i(o)}$ and $B_n^{i(o)}$

Schrödinger's equation in the three regions described above employing the Floquet ansatz. First we consider the region $|x| > L/2$ and find an analytical expression for the wavefunction as follows

$$\psi = \begin{pmatrix} 1 \\ S_{\pm}(E) \end{pmatrix} e^{\pm ik_x x + ik_y y + ik_z z}, \quad (5)$$

where $S_{\pm}(E) = \frac{t(\pm k_x + ik_y)}{E - t_m k_z + s t_z k_z \sin k_0}$ and E represents the incident energy. In order to obtain the wavefunction for the potential region $-L/2 \leq x \leq L/2$, we replace E with $E - V_0$. This results in the substitution of k_x and $S_{\pm}(E)$ respectively by q_x and $S'_{\pm}(E) = S_{\pm}(E - V_0)$ within the above region. Solving the Schrödinger equation we find that the wavefunctions for all spatial regions are

are the amplitudes of the incoming (outgoing) waves, associated with n -th channel, at the left and right boundaries of the well.

From fundamental quantum mechanical considerations, we demand continuity and differentiability of the wave function at the boundaries of the driving potential. This will allow us to relate the incoming amplitudes with the outgoing amplitudes via the intermediate a_n and b_n amplitudes. The detailed derivation on boundary condition is given in Appendix A. We proceed with the construction of the scattering matrix S . The scattering matrix is defined as [66],

$$\begin{pmatrix} A^o \\ B^o \end{pmatrix} = \begin{pmatrix} R & T' \\ T & R' \end{pmatrix} \begin{pmatrix} A^i \\ B^i \end{pmatrix} = S \begin{pmatrix} A^i \\ B^i \end{pmatrix} \quad (7)$$

where A^i and B^i represent the amplitudes of the incident waves and A^o and B^o represent the amplitudes of the outgoing signal. The reflection (R, R') and transmission (T, T') sectors of the S matrix can be represented as [65]

$$\begin{pmatrix} R & T' \\ T & R' \end{pmatrix} = \begin{pmatrix} r_{00} & r_{01} & \dots & t'_{00} & t'_{01} & \dots \\ r_{10} & r_{11} & \dots & t'_{10} & t'_{11} & \dots \\ \vdots & \vdots & \dots & \vdots & \vdots & \dots \\ \vdots & \vdots & \dots & \vdots & \vdots & \dots \\ t_{10} & t_{11} & \dots & r'_{10} & r'_{11} & \dots \\ t_{10} & t_{11} & \dots & r'_{10} & r'_{11} & \dots \\ \vdots & \vdots & \dots & \vdots & \vdots & \dots \\ \vdots & \vdots & \dots & \vdots & \vdots & \dots \end{pmatrix}, \quad (8)$$

where r_{nm} and t_{nm} are reflection and transmission amplitudes for modes incident from the left and r'_{nm} and t'_{nm} are reflection and transmission amplitudes for modes incident from the right. The detailed derivation on S -matrix formulation is given in Appendix B. Here, we have $n, m \in (0, \infty)$ since only propagating modes are considered. Note that we consider only one incoming electron of energy E i.e., there exist only one incoming channel. Hence, we work with $n = 0$ case only. From the S matrix, we can define the total transmission coefficient T as [60, 64, 65]

$$T = \sum_{m=0}^{\infty} \frac{\text{Re}(k_0)}{\text{Re}(k_m)} |t_{0m}|^2. \quad (9)$$

IV. RESULTS

We now proceed with the numerical evaluation of the transmission coefficient (T) and reflection coefficient (R) from the S -matrix. In all cases, we ensure that $R+T = 1$.

We investigate the Fano resonance profile with the incident energy E by keeping k_z fixed and varying k_y in Figs. 2 and 3 for positive and negative chiralities, respectively. We further explore the Fano resonance characteristics by keeping k_y fixed and varying k_z in Figs. 4 and 5 for positive and negative chiralities, respectively. These investigations help us understand the tilt-mediated Fano resonance profile along the direction of tilt momentum and perpendicular to it. In all the above scenarios, we consider two sets of values $(\phi_1, \phi_2) = (\pi/4, \pi/2)$ and $(\phi_1, \phi_2) = (\pi, \pi/2)$ such that effect of the tilt is extensively analyzed. For our numerical computation, we choose $k_0 = \pi/2$, $t = t_z = 1$ and $s = \pm 1$, without the loss of generality. For $\phi_1 = \pi/4$ and $\phi_2 = \pi/2$, we obtain $\eta_{\pm} = |\sqrt{2}t_1 \pm 2\sqrt{2}t_2|$. We find $\eta_{\pm} = |4t_2 \mp 2t_1|$ for $\phi_1 = \pi$ and $\phi_2 = \pi/2$. We now choose appropriate values of t_1 and t_2 such that we are able to probe all phases of the WSM model. We reiterate that $\eta_{\pm} < 1$ represent type-I WSMs, and $\eta_{\pm} > 1$ represent type-II WSMs. Notice that $t_{1,2}$ are key parameters responsible for tilted spectrum even in the absence of $\phi_{1,2}$ i.e., $\phi_{1,2} = 0$.

The harmonically driven potential well leads to the formation of quasi-bound states, associated with the system of interest, inside the well which are absent for the static potential well. The underlying physics of Fano resonances appearing in the transmission T spectrum can be understood in terms of the quasi-bound state energies of the system inside the driven potential well. When the energy difference between the incident beam and the quasi-bound state energy is an integer multiple of $\hbar\omega$ (the photon energies), an electron can be absorbed into the quasi-bound state or an electron can be emitted from the quasi-bound state. The Floquet sidebands, caused by the periodic driving of the well, participate in the above virtual processes thus giving rise the quasi-bound states for the WSM that are localized inside the well. In the transmission spectrum, the Fano resonances are associated with the structures where a sharp dip appears following a sharp peak or vice-versa. In what follows, we are interested in the distribution of the Fano resonances as we vary the different parameters described above.

In all cases, we work with the natural units $\hbar = c = e = k_B = 1$. We consider one Floquet sideband around the zero photon-sector in our numerical analysis that is sufficient to achieve numerical accuracy with a finite termination of the infinite sum. Note that $V_1/\omega \ll 1$ in our analysis. We consider incident energy, potential barrier height, and frequency all in the unit of 10^{-3} eV. The fermi velocities t, t_z and tilt strength $t_{1,2}$ are measured in the unit of 10^6 m/s. The momenta $k_{y,z}$ are considered in the unit of $(10^{-9} \text{ m})^{-1}$. The length of the potential barrier L is the unit of 10^{-9} m.

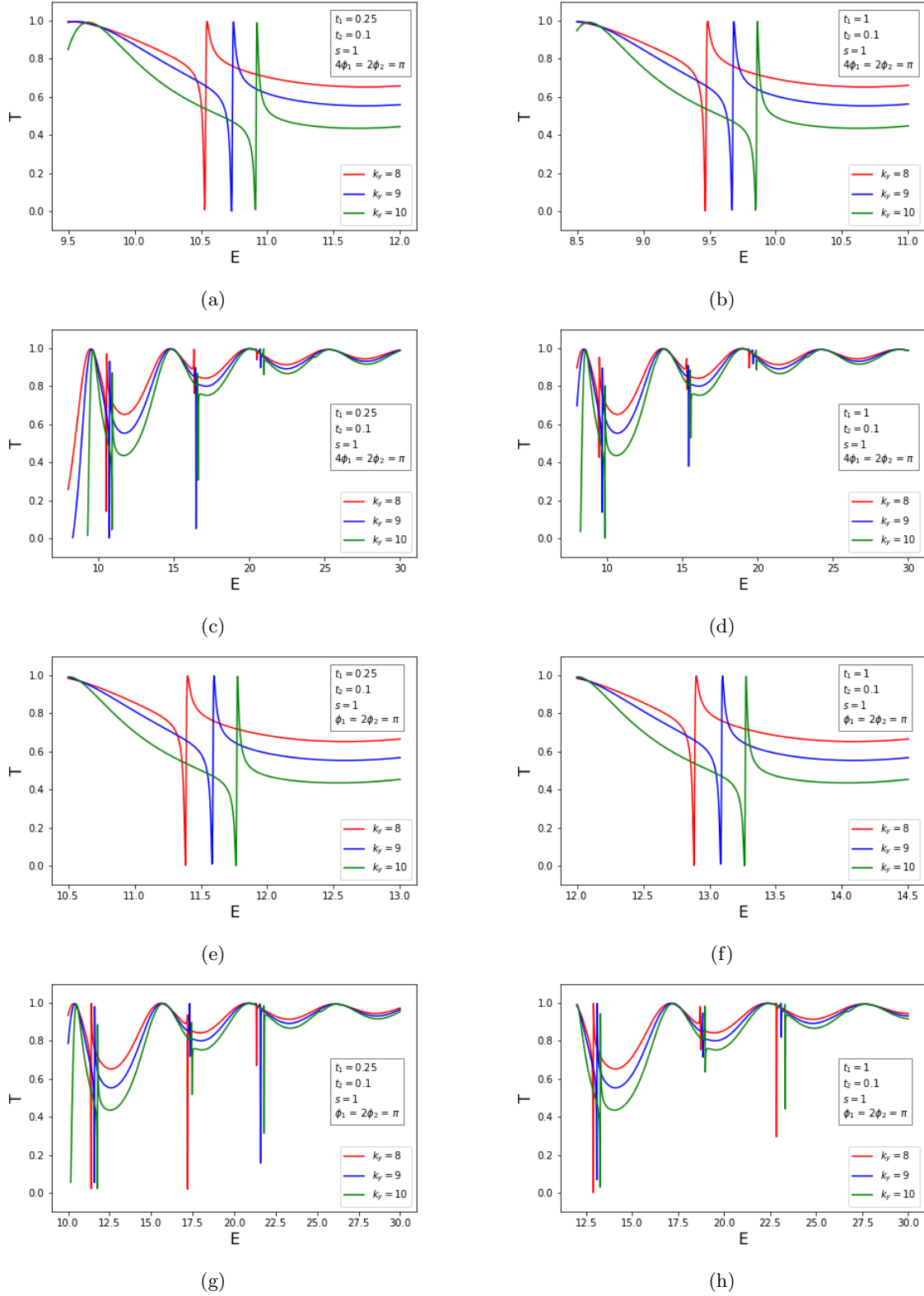


FIG. 2: Transmission spectra T , computed from Eq. (9), as a function of incident energy E for positive chirality Weyl point with $s = +1$ are shown above keeping k_z fixed while changing value of k_y . Here (a,b) depict first Fano resonance and (c,d) show a large region of incident energy region for $\phi_1 = \pi/4$ and $\phi_2 = \pi/2$. We repeat (a,b) and (c,d) in (e,f) and (g,h), respectively for $\phi_1 = \pi$ and $\phi_2 = \pi/2$. Parameters are taken as follows $L = 0.6$, $k_z = 1$, $V_0 = 100$, $V_1 = 0.5$ and $\omega = 15$.

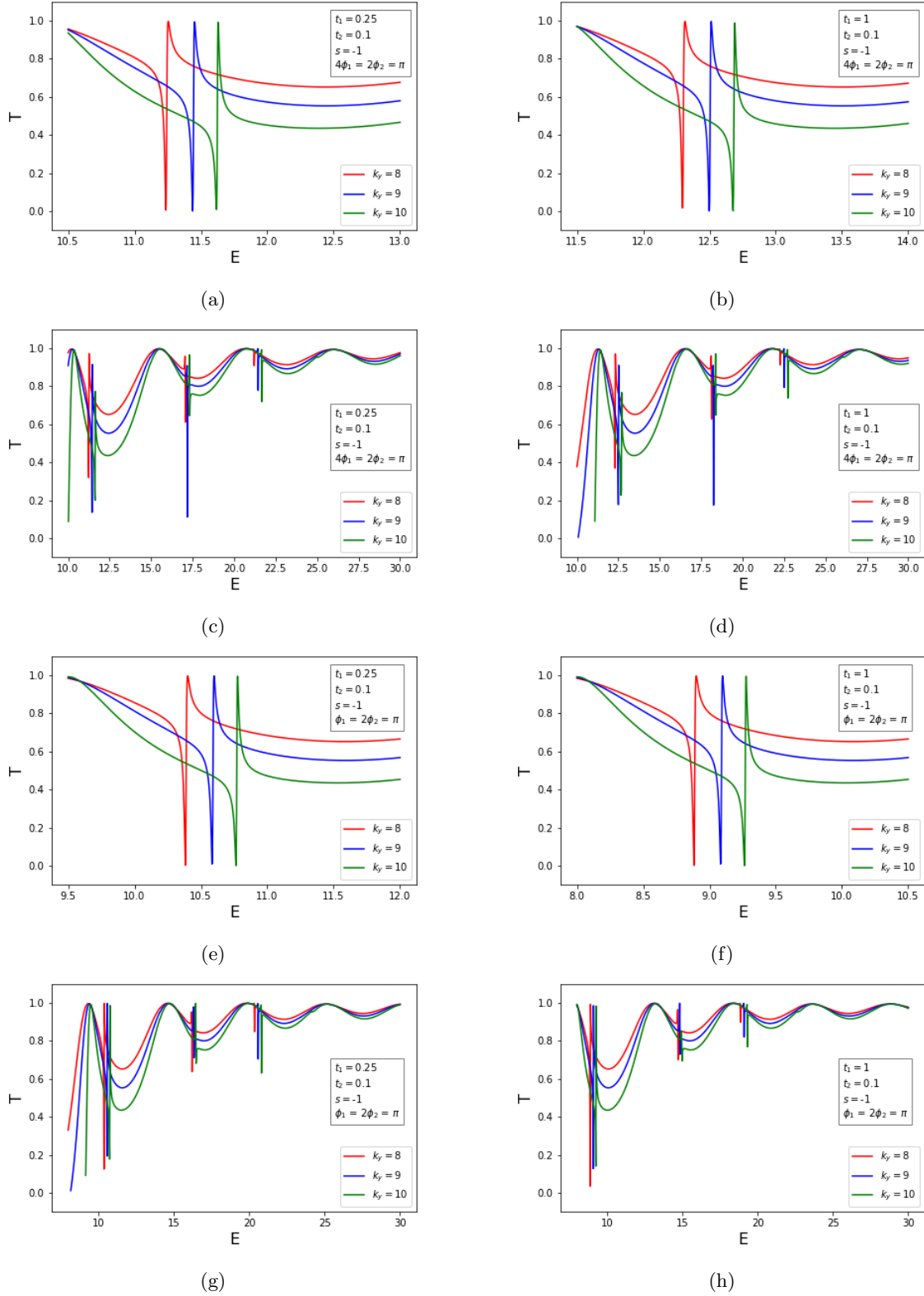


FIG. 3: We repeat Fig. 2 for negative chirality Weyl point with $s = -1$

A. Case 1: Fixed k_z and varying k_y

We here examine the evolution of the transmission spectra in Figs. 2 and 3 for $s = 1$ and -1 , respectively,

when the tilt factor t_1 increases such that we encounter type-I and type-II WSM phases. The details of the Fano resonance energies are given in table I.

| (ϕ_1, ϕ_2) | s | t_1 | 1 st Fano Resonance Energy | | | η_s |
|--------------------|-----|-------|---------------------------------------|------------|------------|----------|
| | | | $k_y = 8$ | $k_y = 10$ | $k_y = 12$ | |
| $(\pi/4, \pi/2)$ | 1 | 0.25 | 10.54 | 10.74 | 10.92 | 0.6364 |
| | | 1 | 9.48 | 9.68 | 9.86 | 1.6971 |
| | -1 | 0.25 | 11.24 | 11.44 | 11.62 | 0.0707 |
| | | 1 | 12.31 | 12.51 | 12.68 | 1.1314 |
| $(\pi, \pi/2)$ | 1 | 0.25 | 11.39 | 11.60 | 11.77 | 0.1 |
| | | 1 | 12.89 | 13.09 | 13.27 | 1.6 |
| | -1 | 0.25 | 10.39 | 10.59 | 10.77 | 0.9 |
| | | 1 | 8.89 | 9.09 | 9.27 | 2.4 |

TABLE I: We tabulate the energies associated with Fano resonances for case 1. We choose $k_z = 1$.

The Fano resonances for the larger k_y appears at greater values of incident energy E irrespective of the choice of the parameters $\phi_{1,2}$, $t_{1,2}$ and chiralities $s = \pm 1$ as clearly observed by scrutinizing the first Fano resonance in Figs. 2 (a,b,e,f) and 3 (a,b,e,f). However, we observe significant differences between the cases $s = 1$ and $s = -1$ as described below. The Fano resonance energy decreases with t_1 for the $s = 1$ case and increases with the increase in t_1 in $s = -1$ case, for $(\phi_1, \phi_2) = (\pi/4, \pi/2)$. An exact opposite trend is noticed for $(\phi_1, \phi_2) = (\pi, \pi/2)$ case. The underlying physics is explained by noting that varying the tilt alters the energies of the Floquet quasi-bound states, which leads to changes in the energetics of the Fano resonances - hence they appear at different points as a function of tilt. It is extremely difficult to obtain a closed form of expression of the quasi-bound state energy, however, one can anticipate the tilt dependence in the above quantity same as the tilt term in energy of the bare Hamiltonian. Importantly, the quasi-bound state energies for the untilted and the tilted case differ by the tilt term precisely.

Examining the first Fano resonance at energy E_F^1 further, we find that the Fano resonance energy linearly increases with increasing k_y irrespective of the chirality of the node and tilt strength. This causes the gap between Fano resonance energies, occurring for two different values of k_y , to become constant irrespective of the choice of parameters $\phi_{1,2}$, $t_{1,2}$ and chiralities $s = \pm 1$. This clearly conveys that the tilt-mediated part in the quasi-bound state energy is not a function of k_y . One can decompose the quasi-bound state energy in two parts where the tilt-mediated part vanishes if $t_{1,2} = 0$ while the other untilted part remains non-zero even if $t_{1,2} = 0$. This is qualitatively similar to the static case Eq. (3) where $t_{1,2}$ are responsible for the tilt even in the absence of $\phi_{1,2}$. Importantly, the k_y -dependency is solely coming from the untilted part of the quasi-bound state energy. This is also similar to the case of the static energy dispersion where

the untilted part only depends on k_y while the tilted part is independent of k_y .

Interestingly, the tilt-mediated part in the quasi-bound state energy is a function of $t_{1,2}$, $\phi_{1,2}$ and chirality leading to a change in quasi-bound state energy with all the above parameters while k_y is still kept fixed. This causes the Fano resonance energies to shift with all the above parameters [see Figs. 2 (a,b,e,f) and 3 (a,b,e,f)]. One can compute the tilt term $2k_z(-st_1 \cos \phi_1 - 2t_2 \sin \phi_2)$, provided $k_0 = \pi/2$, from the static energy dispersion for all the above parameters to find an quantitative agreement with the shift in the Fano resonance energy. For example, the tilt term in the static case becomes more negative [positive] when t_1 increases for $(\phi_1, \phi_2) = (\pi/4, \pi/2)$ [$(\pi, \pi/2)$] and $s = +1$. On the other hand, untilted part of quasi-bound state energy remains unaltered as it is independent of the tilt parameters $t_{1,2}$, $\phi_{1,2}$. Therefore, the quasi-bound state energy will be shifted by the exact amount as the tilted part of the static energy changes, demonstrated in Fig. 2 (a,b,e,f). This correlation can be further verified for $s = -1$ with $(\phi_1, \phi_2) = (\pi/4, \pi/2)$ [$(\pi, \pi/2)$] where static tilt term increases in the positive [negative] energy side causing the Fano resonance energy to increase [decrease] with t_1 (see Fig. 3 (a,b,e,f)). One could expect all the above findings to be qualitatively remained if t_2 is varied while keeping t_1 fixed as the tilt term involves t_1 and t_2 both. Therefore, tilt-mediated part of the quasi-bound energy states are exactly given by the static counterpart while the untilted part of the earlier quantity is extremely hard to compute analytically.

We depict the follow-up Fano resonances namely higher Fano resonances, appearing at higher incident energies E_F^n with $n > 1$ after the first Fano resonance, for both the chiralities in Figs. 2 (c,d,g,h) and 3 (c,d,g,h). We notice that the energy gap between two consecutive Fano resonances always decreases for a given value of k_y when the incident energy becomes higher. This is essentially caused by the fact that the quasi-bound state energies are not equispaced rather the energy gap between them decreases. These quasi-bound state energy levels inside the potential well are taking part in the virtual photon transfer process with the incident beam. The dip-peak structure in the following Fano resonances can be reversed as compared to the first Fano resonance. We note that since there is no Fermi surface based phenomena in this scattering analysis even if we increase the tilt strength, our results do not distinguish between the type-I and type-II phases of WSM. The underlying physics is governed by the tilt altering the energies of the Floquet quasi-bound states, which leads to the changes in the energetics of the Fano resonances. As a result, they appear at different points as a function of tilt.

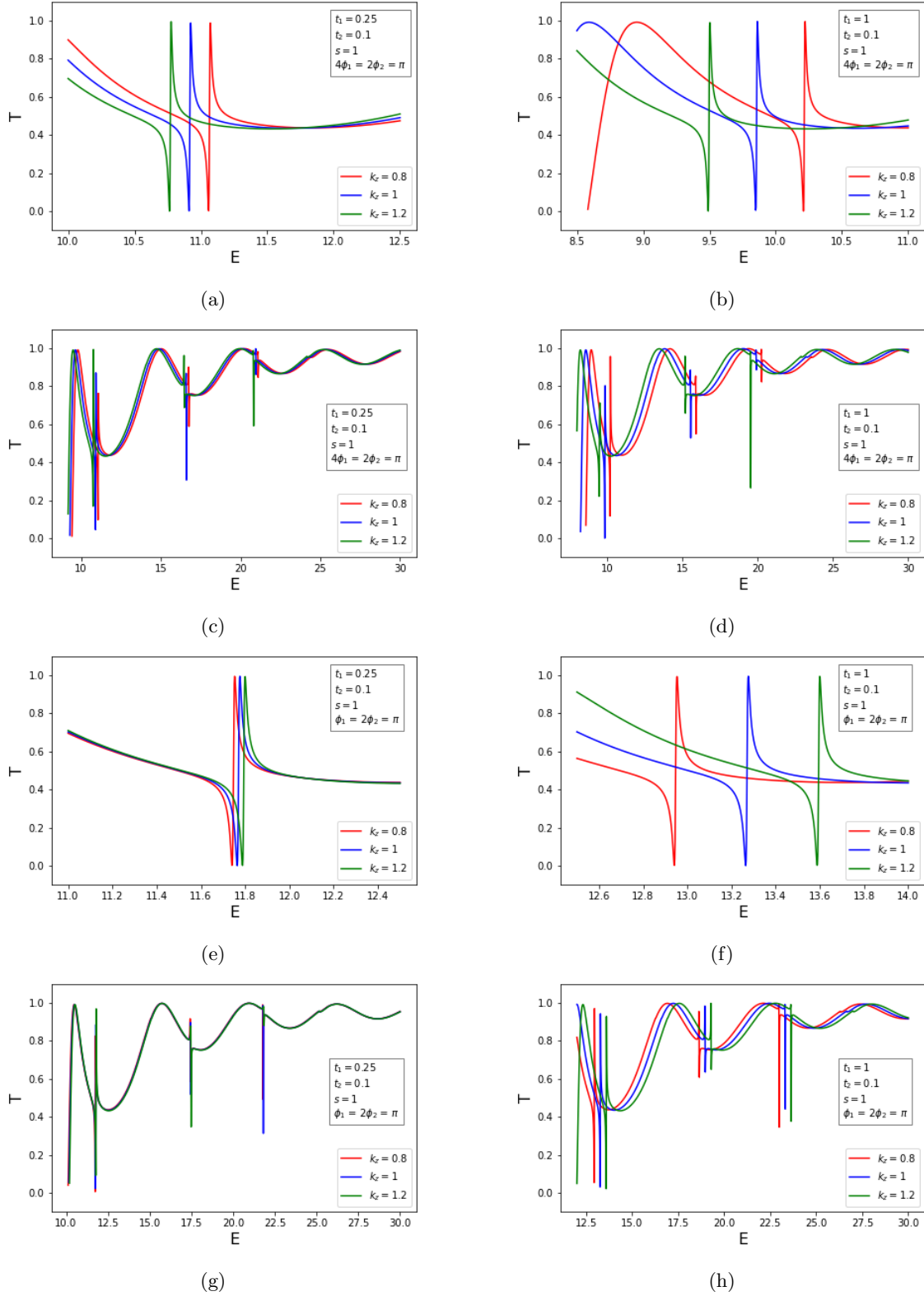


FIG. 4: Transmission spectra T , computed from Eq. (9), as a function of incident energy E for positive chirality Weyl point with $s = +1$ are shown above keeping k_y fixed while changing value of k_z . Here (a,b) display the first Fano resonance and (c,d) show a large energy region of incident energy for $\phi_1 = \pi/4$ and $\phi_2 = \pi/2$. We repeat (a,b) and (c,d) in (e,f) and (g,h), respectively for $\phi_1 = \pi$ and $\phi_2 = \pi/2$. Parameters are taken as follows $L = 0.6$, $k_z = 1$, $V_0 = 100$, $V_1 = 0.5$ and $\omega = 15$.

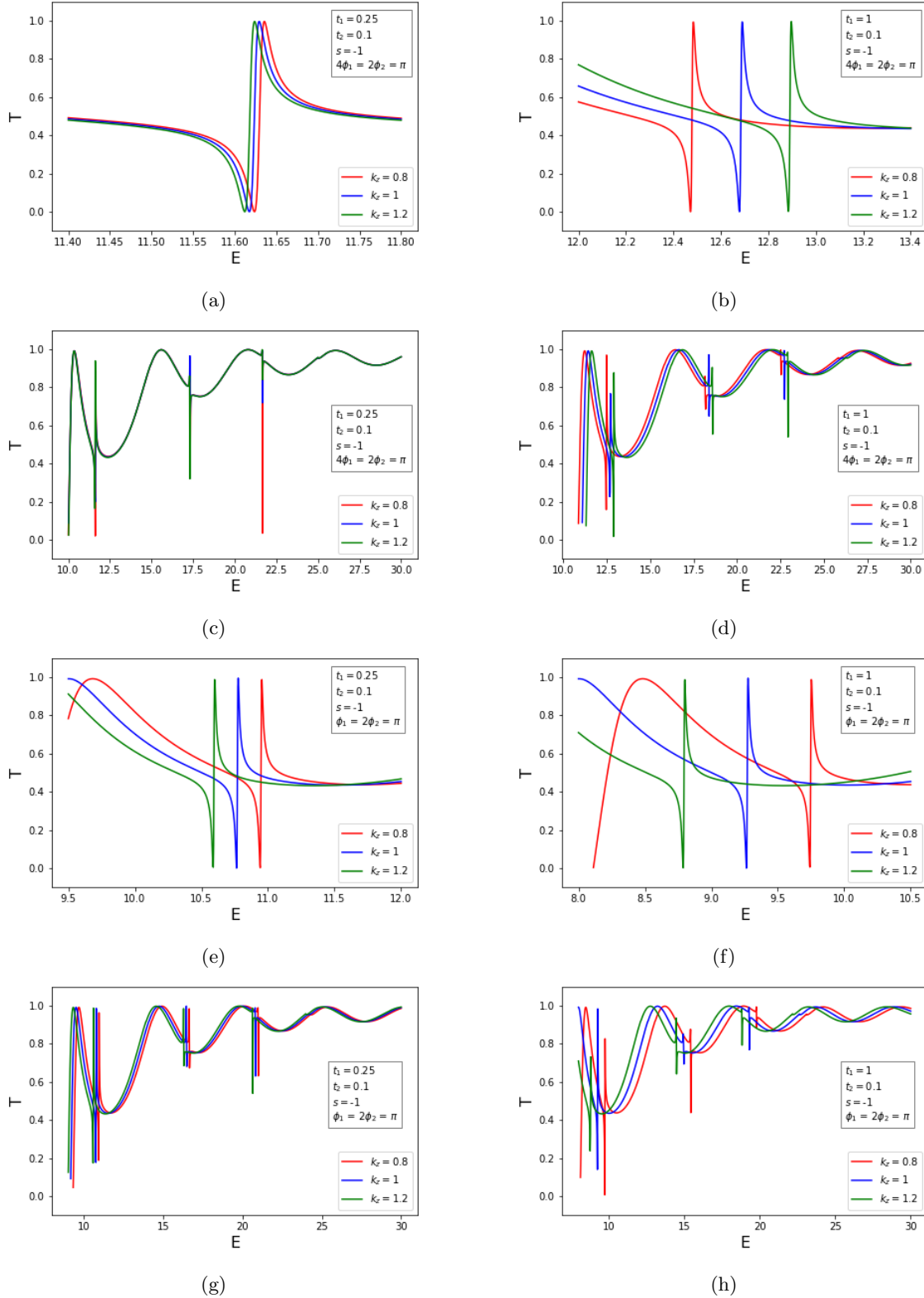


FIG. 5: We repeat Fig. 4 for negative chirality Weyl point with $s = -1$.

B. Case 2: Fixed k_y and varying k_z

Similar to the earlier section, we here examine the evolution of the transmission spectra in Figs. 4 and 5 for

$s = 1$ and -1 , respectively, when the tilt factor t_1 increases. The Fano resonance energies are listed in table II. The first Fano resonance energy E_F^1 , corresponding

to positive chirality, decreases [increases] with increasing t_1 with a given value of k_z for $(\phi_1, \phi_2) = (\pi/4, \pi/2)$ $[(\pi, \pi/2)]$ as depicted in Figs. 4 (a,b,e,f). The situation is reversed for negative chirality as shown in Figs. 5 (a,b,e,f). This feature is also observed in the previous case. On the other hand, the marked difference for the present case is the following: the energy gap between two successive Fano resonances, associated with two different values of the tilt momentum k_z , varies with increasing t_1 . This energy gap also changes if one changes the chirality as well as $\phi_{1,2}$. This suggests that the tilt-mediated part in the quasi-bound state energy depends on k_z , $t_{1,2}$, $\phi_{1,2}$ and s . This can be quantitatively understood from the tilted part in the static energy dispersion Eq. (3). As discussed earlier, the untilted part of the quasi-bound state energy is independent of $t_{1,2}$, $\phi_{1,2}$ and s . The tilt momentum k_z appears both in the tilted as well as untilted part of the above energy. Therefore, once we vary all the parameters $t_{1,2}$, and $\phi_{1,2}$ including k_z for a given chirality, both the untilted and tilted-mediated parts in the quasi-bound state energy change in a non-trivial manner.

The above phenomena leads to a rich Fano resonance profile that is an admixture of effects coming from tilt factors $t_{1,2}$ and tilt momentum k_z simultaneously. This can be further understood from the fact that beyond a certain value of t_1 the order of the Fano resonance with k_z changes i.e., quasi-bound state energies increase (decrease) with increasing k_z instead of decrease (increase). This is noticed in Fig. 5 (a,b). Therefore, the appearance of Fano resonances with k_z is relative to the choice of the parameters such as $t_{1,2}$, and $\phi_{1,2}$. One could expect similar findings if t_2 is varied while keeping t_1 fixed as the tilt term involves t_1 and t_2 both. A careful investigation suggests that the Fano resonance energy changes linearly with increasing k_z (t_1) for a given value of t_1 (k_z). This causes the energy separation between two subsequent Fano resonances to vary linearly with increasing the product of t_1 and k_z . This collective behavior indicates that tilt-mediated part of the quasi-bound state energies behave in a qualitatively different manner as compared to the untilted counterpart.

| (ϕ_1, ϕ_2) | s | t_1 | 1 st Fano Resonance Energy | | | η_s |
|--------------------|----|-------|---------------------------------------|------------|------------|----------|
| | | | $k_y = 8$ | $k_y = 10$ | $k_y = 12$ | |
| $(\pi/4, \pi/2)$ | 1 | 0.25 | 11.06 | 10.92 | 10.77 | 0.6364 |
| | | 1 | 10.21 | 9.85 | 9.49 | 1.6971 |
| | -1 | 0.25 | 11.63 | 11.62 | 11.61 | 0.0707 |
| | | 1 | 12.48 | 12.68 | 12.89 | 1.1314 |
| $(\pi, \pi/2)$ | 1 | 0.25 | 11.75 | 11.77 | 11.79 | 0.1 |
| | | 1 | 12.94 | 13.26 | 13.59 | 1.6 |
| | -1 | 0.25 | 11.32 | 11.52 | 11.69 | 0.9 |
| | | 1 | 9.74 | 9.26 | 8.79 | 2.4 |

TABLE II: We tabulate the energies of the Fano resonance for case 2. We fix $k_y = 10$.

We now turn our attention to the follow-up Fano res-

onance at energies E_F^n with $n > 1$ profiles when the incident energy increases as shown in Figs. 4 (c,d,g,h) and 5 (c,d,g,h) for positive and negative chiralities, respectively. Similar to the earlier section, we find that the energy gap between two successive higher Fano resonances decreases with increasing the incident energy for a given value of k_z . Such repeated occurrence of Fano resonances with a variation in the dip-peak structures is commonly visible when t_1 increases as expected. The existence of multiple quasi-bound states with unequal energy spacing can be inferred as well from the above findings.

V. DISCUSSION

We plot the incident energies E_F^1 , corresponding to the first Fano resonance, as a function of t_1 keeping k_y as a parameter (see Fig. 6). We investigate the case of $(\phi_1, \phi_2) = (\pi/4, \pi/2)$ $[(\pi, \pi/2)]$ in Fig. 6 (a,b) $[(c,d)]$. We repeat the Fig. 6 with k_z as a parameter in Fig. 7. The linear behavior of Fano resonance energy with t_1 infers that the quasi-bound state energy varies linearly with t_1 . This further boils down to the fact that the tilt-mediated part shows linear dependence with t_1 . The parallel straight lines, on the other hand, for different values of k_y suggests that the quasi-bound state energies change in an identical manner with k_y irrespective of the values of t_1 . This is in accordance with the fact that tilt-mediated part of quasi-bound state energy does not depend on k_y . Interestingly, the untilted part of the above energy is expected to vary linearly with k_y as evident from the equidistant parallel lines. The parallel nature of the straight lines confirms that the energies of the quasi-bound state do not involve any product term $t_1 k_y$, rather it depends on k_y and t_1 separately.

The positive and negative slopes of these parallel lines denote the coefficient in front of these energies that depend on chirality as well as the choice of $\phi_{1,2}$. We find the sign of the coefficient reverses as chirality switches its sign while $\phi_{1,2}$ are kept fixed. The change in the sign of chirality $s = 1$ to $s = -1$ can alter the sign of the slopes of these straight lines without affecting their parallel nature. This further suggests that energies depends on the product of st_1 while k_y does not couple with s . One can understand all the above findings by analyzing the tilt term $2k_z(-st_1 \cos \phi_1 - 2t_2 \sin \phi_2)$ in the static energy dispersion with a given set of parameters.

Examining Figs. 7 in details, we find that the first Fano resonance energy E_F^1 changes linearly with tilt parameter t_1 while the slope depends on k_z . This results in intersecting straight lines for different values of k_z unlike the previous case of parallel lines in Fig. 6. On the other hand, these energies also depend linearly on k_z given a fixed value of t_1 . Interestingly, for certain values of t_1 , the Fano resonance energies for different values of k_z become identical. This equi-energy point changes to a different value of t_1 once t_2 and/or the chirality s changes for a fixed parameter set of $\phi_{1,2}$. This refers

to the fact that there exist an additional $t_2 k_z$ tilt term in the energy, and can be clearly understood from the tilt term $2k_z(-st_1 \cos \phi_1 - 2t_2 \sin \phi_2)$ of the static model. The intersection point is observed when the tilt-mediated part of the quasi-bound state energy vanishes for a certain set of t_1^* and t_2^* values given $\phi_{1,2}$ fixed. The values of t_1^* , such that $-st_1^* \cos \phi_1 = 2t_2^* \sin \phi_2$, can be exactly computed from the tilt term in the static model.

The non-parallel intersecting nature of the straight lines confirms that energies of the quasi-bound state involve the product term $st_1 k_z$. This collective dependence rules out the individual dependence on k_z and t_1 . The change in the sign of chirality $s = 1$ to $s = -1$, can alter the sign of the slopes of these straight lines without affecting the intersecting nature. The energies linearly change with k_z while the proportionality factor depends on the product of st_1 and t_2 separately as evident from the tilt term in the low-energy Hamiltonian Eq. (1). This describes the intersecting nature of the plots and alteration in order of the Fano resonance peaks with k_z upon changing t_1 across t_1^* keeping all the other parameter fixed, as noticed in Fig. 5 (a,b).

Controlling material parameters in general is consid-

ered tricky in the experimental community as the tilt can easily be intrinsically present in Dirac semimetals and WSMs with linear as well non-linear band dispersion [22]. We, however, point out a few ways in which our results may be tested in a laboratory. Given the fact that uniaxial strain is found to be useful to introduce tilt in the energy dispersion of graphene [67], applying strain can also cause a variation in the tilt of the WSMs. This method relies on altering the spatial and temporal components of the gauge field [68–70] and maybe used to find Fano resonances when driven by a laser field. Another way in which tilt variations appear is through periodic driving, which has been reported to produce type-I and type-II WSMs [71]. Notice that the tilted Dirac dispersion has been predicted to appear in two-dimension for quinoid-type [72] and hydrogenated graphene [73], 8-Pmmn Borophene [74], planar arrays of carbon nanotubes [75]. The tilted Dirac cones have been experimentally observed in the photonic Lieb-kagome lattices [76]. We believe that the above theoretical predictions and experimental techniques will be instrumental in future to engineer the tilted dispersion of WSMs in three-dimension.

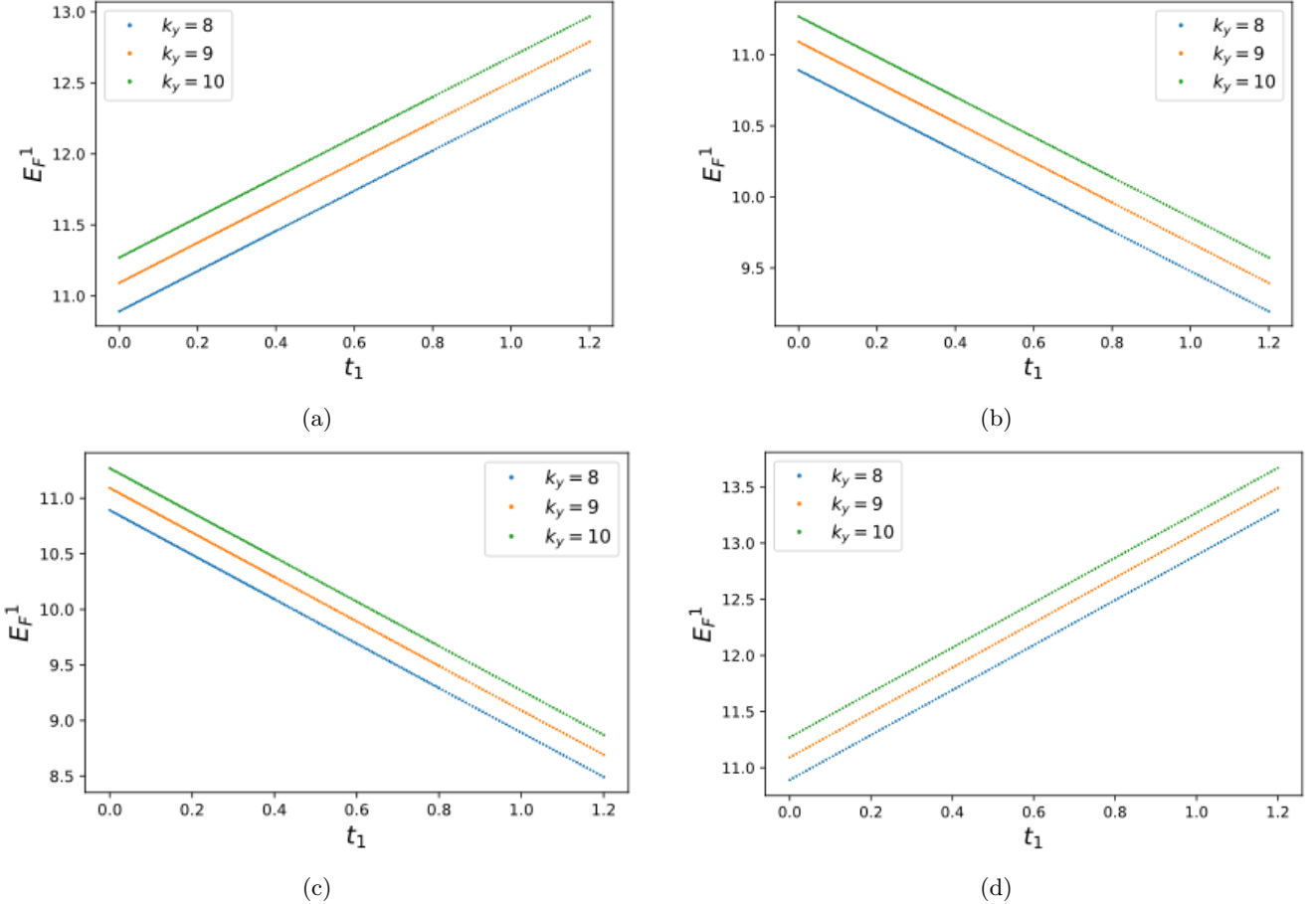


FIG. 6: The energy E_F^1 corresponding to first Fano resonance as found in Figs. 2 and 3, are shown as a function of t_1 . We consider $(\phi_1, \phi_2) = (\pi/4, \pi/2)$ and $(\pi, \pi/2)$ for (a,b) and (c,d), respectively. We choose $s = +1$ and -1 for (a,c) and (b,d), respectively. Parameters are taken as follows $L = 0.6$, $K_y = 10$, $V_0 = 100$, $V_1 = 1$ and $\omega = 15$.

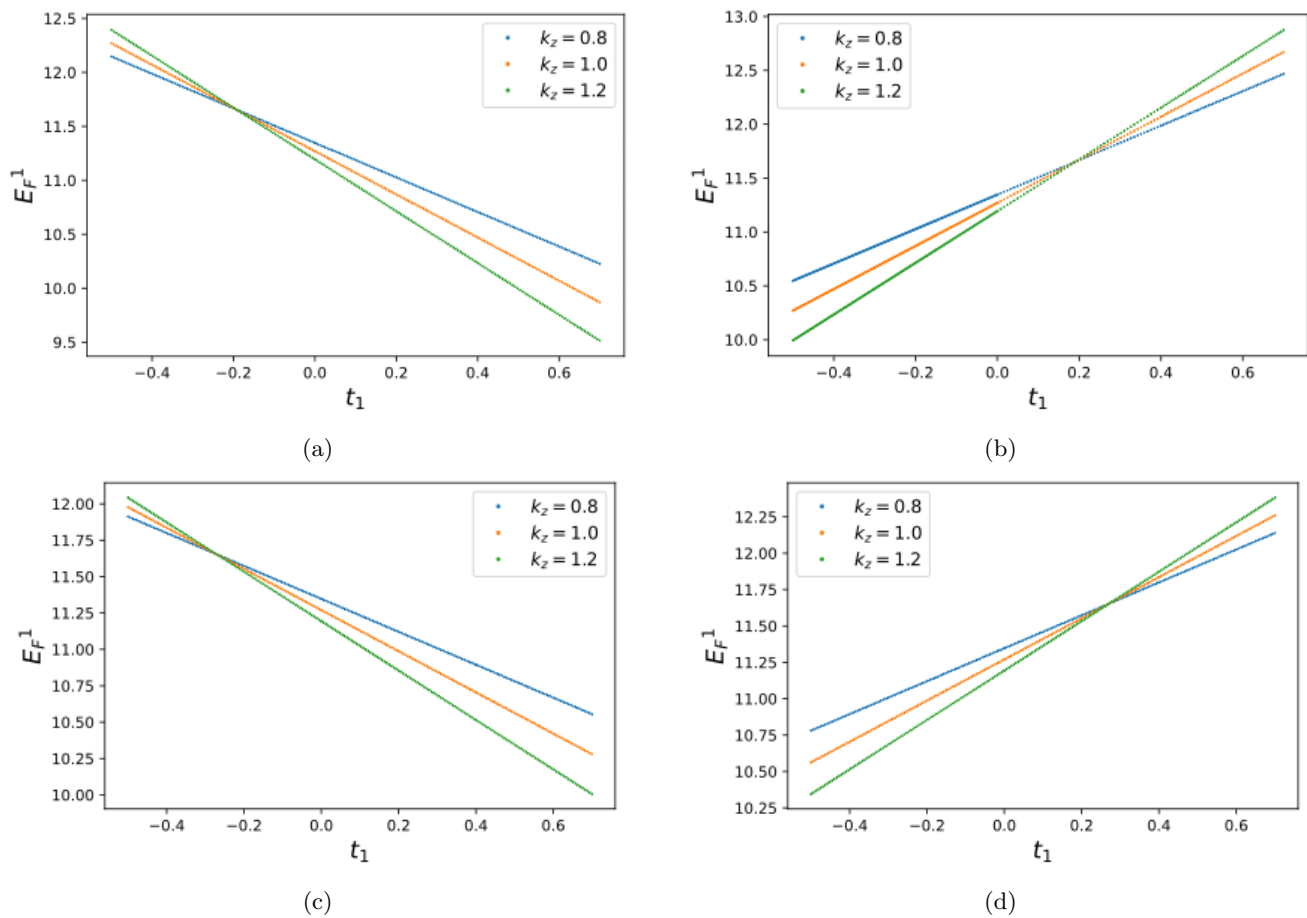


FIG. 7: The energy E_F^1 corresponding to first Fano resonance as found in Figs. 4 and 5, are shown as a function of t_1 . We consider $(\phi_1, \phi_2) = (\pi, \pi/2)$ and $(\pi/4, \pi/2)$ for (a,b) and (c,d), respectively. We choose $s = +1$ and -1 for (a,c) and (b,d), respectively. Parameters are taken as follows $L = 0.6$, $k_y = 10$, $V_0 = 100$, $V_1 = 1$ and $\omega = 15$.

VI. CONCLUSION

In this work, we consider harmonically driven quantum well to study the Fano resonances in tilted WSMs by investigating the transmission spectra using the Floquet scattering theory technique. The potential is oriented in the transverse direction with respect to the tilt allowing us to study the transmission by varying momentum along and perpendicular to the tilt direction. Our study sheds light on the effect of tilt on the Fano resonance where the Fano resonance energy changes linearly with tilt strength. This is caused by the tilt-mediated part of the energy associated with the quasi-bound state residing inside the potential well. For fixed value of the collinear (transverse) momentum with respect to the tilt direction, the energy difference between two Fano resonances, appearing for two adjacent values of transverse (collinear) momentum, does not (does) change with tilt strength. This finding clearly indicates that collinear (transverse) momentum is coupled (decoupled) with tilt strength in the tilt-mediated part of the quasi-bound state energy. The variation of first Fano resonance energy with tilt strength further confirms that the tilt-mediated part of the above

energy is same as the tilt term present in the static energy dispersion. We extensively investigate the evolution of transmission profile with respect to the other tilt parameters and chirality of the Weyl points from which we exact form of the tilt-mediated part is further verified. The normal part of the quasi-energy spectrum is dependent on the collinear as well as the transverse momentum resulting in rich profile of Fano resonance in the parameter space.

Our work thus uncover the complex interplay between the tilt and Fano resonance by probing the tilt-mediated part of quasi-bound state energy even though the closed form of the later itself is not obtainable easily. We believe that our study might play important role in understanding the experimental findings such as currents for periodically driven systems as far as the microscopic mechanisms are concerned. In real mesoscopic systems, the potential region is confined in a finite region of space and hence edge effects are important. Therefore, it would be interesting to study the edge effects in these systems. At the same time, the dynamics of Fano resonance under magnetic field, disorder, interaction and other dephasing mechanism might be important for future studies.

VII. ACKNOWLEDGEMENT

We acknowledge the technical help from Rui Zhu. TN would like to thank Ipsita Mondal for the very initial discussions on the Floquet scattering techniques. TN also thanks Anton Gregefalk for fruitful discussions.

Appendix A: Boundary matching

In this appendix, we discuss the boundary conditions in details for the wave-functions to be continuous across the boundary along with their derivations. This allows us to relate the coefficients A_n , B_n , a_m and b_m as discussed in Sec. III.

At $x = -L/2$ boundary condition,

$$A_n^i N_{n+} e^{-iK_{xn}L/2} + A_n^0 N_{n-} e^{ik_{xn}L/2} = \sum_{m=-\infty}^{\infty} [a_m N'_{m+} e^{-iq_m L/2} + b_m N'_{m-} e^{iq_m L/2}] J_{n-m} \left(\frac{V_1}{\hbar\omega} \right) \quad (\text{A1})$$

$$A_n^i N_{n+} S_+(E_n) e^{-iK_{xn}L/2} + A_n^0 N_{n-} S_-(E_n) e^{ik_{xn}L/2} = \sum_{m=-\infty}^{\infty} [a_m N'_{m+} S'_+(E_m) e^{-iq_m L/2} + b_m N'_{m-} S'_-(E_m) e^{iq_m L/2}] J_{n-m} \left(\frac{V_1}{\hbar\omega} \right) \quad (\text{A2})$$

At $x = L/2$ boundary condition,

$$B_n^i N_{n-} e^{-iK_{xn}L/2} + B_n^0 N_{n+} e^{ik_{xn}L/2} = \sum_{m=-\infty}^{\infty} [a_m N'_{m+} e^{iq_m L/2} + b_m N'_{m-} e^{-iq_m L/2}] J_{n-m} \left(\frac{V_1}{\hbar\omega} \right) \quad (\text{A3})$$

$$B_n^i N_{n-} S_-(E_n) e^{-iK_{xn}L/2} + B_n^0 N_{n+} S'_+(E_n) e^{ik_{xn}L/2} = \sum_{m=-\infty}^{\infty} [a_m N'_{m+} S'_+(E_m) e^{iq_m L/2} + b_m N'_{m-} S'_-(E_m) e^{-iq_m L/2}] J_{n-m} \left(\frac{V_1}{\hbar\omega} \right) \quad (\text{A4})$$

Now, from above equations,

$$A_n^i [S_-(E_n) - S_+(E_n)] e^{-ik_{xn}L/2} = \frac{1}{N_{n+}} \sum_{m=-\infty}^{\infty} [a_m N_{m+} (S_-(E_n) - S'_+(E_m)) e^{-iq_m L/2} + b_m N_{m-} (S_-(E_n) - S'_-(E_m)) e^{iq_m L/2}] J_{n-m} \left(\frac{V_1}{\hbar\omega} \right) \quad (\text{A5})$$

$$B_n^i [S_-(E_n) - S_+(E_n)] e^{-ik_{xn}L/2} = \frac{1}{N_{n-}} \sum_{m=-\infty}^{\infty} [a_m N_{m+} (S'_+(E_m) - S_+(E_n)) e^{iq_m L/2} + b_m N_{m-} (S'_-(E_m) - S_+(E_n)) e^{-iq_m L/2}] J_{n-m} \left(\frac{V_1}{\hbar\omega} \right) \quad (\text{A6})$$

Now we define the matrices as -

$$(M_{sa}^{\pm})_{nm} = N'_{m+} \left[\left(\frac{1}{N_{n+}} \right) (S'_+(E_m) - S_-(E_n)) e^{i(k_{xn} - q_m)L/2} \pm \left(\frac{1}{N_{n-}} \right) (S_+ E_n - S'_+(E_m)) e^{i(k_{xn} + q_m)L/2} \right] J_{n-m} \left(\frac{V_1}{\hbar\omega} \right) \\ (M_{sb}^{\pm})_{nm} = N'_{m-} \left[\left(\frac{1}{N_{n+}} \right) (S'_-(E_m) - S_-(E_n)) e^{i(k_{xn} + q_m)L/2} \pm \left(\frac{1}{N_{n-}} \right) (S_+ E_n - S'_-(E_m)) e^{i(k_{xn} - q_m)L/2} \right] J_{n-m} \left(\frac{V_1}{\hbar\omega} \right) \quad (\text{A7})$$

$$(M_{cA}^1)_{nm} = \frac{N'_{m+}}{N_{n-}} e^{-i(q_m + k_{xn})L/2} J_{n-m} \left(\frac{V_1}{\hbar\omega} \right) \quad (\text{A8})$$

$$(M_{cA}^2)_{nm} = \frac{N'_{m-}}{N_{n-}} e^{i(q_m - k_{xn})L/2} J_{n-m} \left(\frac{V_1}{\hbar\omega} \right) \quad (\text{A9})$$

$$(M_{cB}^1)_{nm} = \frac{N'_{m+}}{N_{n+}} e^{i(q_m - k_{xn})L/2} J_{n-m} \left(\frac{V_1}{\hbar\omega} \right) \quad (\text{A10})$$

$$(M_{cB}^2)_{nm} = \frac{N'_{m-}}{N_{n+}} e^{-i(q_m + k_{xn})L/2} J_{n-m} \left(\frac{V_1}{\hbar\omega} \right) \quad (\text{A11})$$

$$(M_i)_{nm} = \frac{N_{n+}}{N_{n-}} e^{-ik_{xn}L} \delta_{n,m} \quad (\text{A12})$$

$$(M_r)_{nm} = (S_+(E_n) - S_-(E_n)) \delta_{n,m} \quad (\text{A13})$$

Appendix B: Scattering matrix

In this appendix we show the derivation for the S-matrix based on the boundary condition. The scattering matrix is defined as,

$$\begin{pmatrix} A^o \\ B^o \end{pmatrix} = \begin{pmatrix} M_{AA} & M_{AB} \\ M_{BA} & M_{BB} \end{pmatrix} \begin{pmatrix} A^i \\ B^i \end{pmatrix} = S \begin{pmatrix} A^i \\ B^i \end{pmatrix} \quad (\text{B1})$$

Where, A^i and B^i represent the amplitudes of the incident wave and A^o and B^o represent the amplitudes of the outgoing signal and it can be shown that,

$$M_{AA} = M_{cA}^1 a_A + M_{cA}^2 b_A - M_i \quad (\text{B2})$$

$$M_{BA} = M_{cB}^1 a_A + M_{cB}^2 b_A \quad (\text{B3})$$

$$(\text{B4})$$

With,

$$a_A = [(M_{sb}^+)^{-1} M_{sa}^+ - (M_{sb}^-)^{-1} - M_{sa}^-]^{-1} \\ [(M_{sb}^+)^{-1} - (M_{sb}^-)^{-1}] M_r \quad (\text{B5})$$

$$b_A = [(M_{sa}^+)^{-1}M_{sb}^+ - (M_{sa}^-)^{-1} - M_{sb}^-]^{-1} \quad (\text{B6})$$

$$[(M_{sa}^+)^{-1} - (M_{sa}^-)^{-1}]M_r$$

-
- [1] A. A. Burkov, *J. Phys. Condens. Matter* **27**, 113201 (2015).
- [2] B. Yan and C. Felser, *Annu. Rev. Condens. Matter Phys.* **8**, 337 (2017).
- [3] N. P. Armitage, E. J. Mele, and A. Vishwanath, *Rev. Mod. Phys.* **90**, 015001 (2018).
- [4] E. V. Gorbar, V. A. Miransky, I. A. Shovkovy, P. O. Sukhachov, *Low Temperature Physics* **44**, 487 (2018).
- [5] H. Weng, C. Fang, Z. Fang, B. A. Bernevig, and X. Dai, *Phys. Rev. X* **5**, 011029 (2015).
- [6] Huang, S., Xu, S., Belopolski, I. et al., *Nat. Commun.* **6**, 7373 (2015).
- [7] B. Yan and C. Felser, *Annu. Rev. Condens. Matter Phys.* (2017) 8:337-54.
- [8] M. Z. Hasan, S.-Y. Xu, I. Belopolski, and C.-M. Huang, *Annu. Rev. Condens. Matter Phys.* **8**, 289 (2017).
- [9] G. Xu, H. Weng, Z. Wang, X. Dai, and Z. Fang, *Phys. Rev. Lett.* **107**, 186806 (2011).
- [10] C. Fang, M. J. Gilbert, X. Dai, and B. A. Bernevig, *Phys. Rev. Lett.* **108**, 266802 (2012).
- [11] A. A. Soluyanov, D. Gresch, Z. Wang, Q. Wu, M. Troyer, X. Dai, and B. A. Bernevig, *Nature* **527**, 495-498 (2015).
- [12] G. Autes, D. Gresch, M. Troyer, A. A. Soluyanov, and O. V. Yazyev, *Phys. Rev. Lett.* **117**, 066402 (2016).
- [13] M.-Y. Yao, N. Xu, Q. S. Wu, G. Autes, N. Kumar, V. N. Strocov, N. C. Plumb, M. Radovic, O. V. Yazyev, C. Felser, J. Mesot, and M. Shi, *Phys. Rev. Lett.* **122**, 176402 (2019).
- [14] H. Nielsen and M. Ninomiya, *Phys. Lett. B* **130**, 389 (1983).
- [15] T. Nag, S. Nandy, *J. Phys.: Condens. Matter* **33** (2021) **075504**.
- [16] B. Sadhukhan, T. Nag, *Phys. Rev. B* **107**, L081110 (2023).
- [17] A. Menon and B. Basu, *J. Phys.: Condens. Matter* **33** 045602 (2021).
- [18] F. Xiong, C. Honerkamp, D. M. Kennes, T. Nag, *Phys. Rev. B* **106**, 045424 (2022).
- [19] S. K. Das, T. Nag, S. Nandy, *Phys. Rev. B* **104**, 115420 (2021).
- [20] B. Sadhukhan, T. Nag, *Phys. Rev. B* **103**, 144308 (2021).
- [21] B. Sadhukhan, T. Nag, *Phys. Rev. B* **104**, 245122 (2021).
- [22] T. Nag, D. M. Kennes, *Phys. Rev. B* **105**, 214307 (2022).
- [23] T. E. O. Brien, M. Diez, C. W. J. Beenakker, *Phys. Rev. Lett.* **116**, 236401 (2016).
- [24] Zyuzin, A.A., Tiwari, R.P., *JETP Lett.* **103**, 717-722 (2016).
- [25] Maximilian Trescher, Björn Sbierski, Piet W. Brouwer, and Emil J. Bergholtz, *Phys. Rev. B* **91**, 115135 (2015).
- [26] T. Oka and H. Aoki, *Physical Review B* **79**, 081406(R) (2009).
- [27] T. Kitagawa, E. Berg, M. Rudner, and E. Demler, *Phys. Rev. B* **82**, 235114 (2010).
- [28] M. S. Rudner, N. H. Lindner, E. Berg, and M. Levin, *Phys. Rev. X* **3**, 031005 (2013).
- [29] F. Nathan and M. S. Rudner, *New Journal of Physics* **17**, 125014 (2015).
- [30] P. Titum, E. Berg, M. S. Rudner, G. Refael, and N. H. Lindner, *Phys. Rev. X* **6**, 021013 (2016).
- [31] T. Nag, S. Roy, A. Dutta, D. Sen, *Phys. Rev. B* **89**, 165425 (2014).
- [32] T. Nag, R-J Slager, T. Higuchi, T. Oka, *Phys. Rev. B* **100**, 134301 (2019).
- [33] L. Tamang, T. Nag, T. Biswas, *Phys. Rev. B* **104**, 174308 (2021).
- [34] T. Nag, A. Rajak, *Phys. Rev. B* **104**, 134307 (2021).
- [35] A. Kundu, A. Rajak, T. Nag, *Phys. Rev. B* **104**, 075161 (2021).
- [36] H. C. Po, L. Fidkowski, T. Morimoto, A. C. Potter, and A. Vishwanath, *Phys. Rev. X* **6**, 041070 (2016).
- [37] S. Kar and B. Basu, *Phys. Rev. B* **98**, 245119 (2018).
- [38] J. H. Shirley, *Phys. Rev.* **138**, B979 (1965).
- [39] M. Holthaus and D. Hone, *Phys. Rev. B* **47**, 6499 (1993).
- [40] T. Fromherz, *Phys. Rev. B* **56**, 4772 (1997).
- [41] A. Menon, D. Chowdhury, and B. Basu, *Phys. Rev. B* **98**, 205109 (2018).
- [42] T. Nag, A. Menon, and B. Basu, *Phys. Rev. B* **102**, 014307 (2020).
- [43] Zhang, B., Maeshima, N., and Hino, Ki., *Sci. Rep.* **11**, 2952 (2021).
- [44] Kumar, U., Banerjee, S., and Lin, S.Z., *Nat. Commun. Phys.* **5**, 157 (2022).
- [45] U. Fano, *Nuovo Cimento* **12**, 154 (1935).
- [46] A. E. Miroshnichenko, S. Flach, and Y. S. Kivshar, *Rev. Mod. Phys.* **82**, 2257 (2010).
- [47] B. Lukyanchuk, N. I. Zheludev, S. A. Maier, N. J. Halas, P. Nordlander, H. Giessen, and C. T. Chong, *Nat. Mater.* **9**, 707 (2010).
- [48] E. Tekman and P. F. Bagwell, *Phys. Rev. B* **48**, 2553 (1993).
- [49] H. G. Luo, T. Xiang, X. Q. Wang, Z. B. Su, and L. Yu, *Phys. Rev. Lett.* **92**, 256602 (2004).
- [50] A. C. Johnson, C. M. Marcus, M. P. Hanson, and A. C. Gossard, *Phys. Rev. Lett.* **93**, 106803 (2004).
- [51] B. R. Bulka and P. Stefanski, *Phys. Rev. Lett.* **86**, 5128 (2001).
- [52] M. E. Torio, K. Hallberg, S. Flach, A. E. Miroshnichenko, and M. Titov, *Eur. Phys. J. B* **37**, 399 (2004).
- [53] C. S. Chu and R. S. Sorbello, *Phys. Rev. B* **40**, 5941 (1989).
- [54] R. Zhu, *J. Phys.: Condens. Matter* **25**, 036001 (2013).
- [55] T. B. Boykin, B. Pezeshki, and J. S. Harris, *Phys. Rev. B* **46**, 12769 (1992).
- [56] W. Porod, Z. Shao, and C. S. Lent, *Appl. Phys. Lett.* **61**, 1350 (1992).
- [57] J. L. Cardoso and P. Pereyra, *Europhys. Lett.* **83**, 38001 (2008).
- [58] K. Kobayashi, H. Aikawa, A. Sano, S. Katsumoto, and Y. Iye, *Phys. Rev. B* **70**, 035319 (2004).
- [59] R. Zhu and M. Liu, *Eur. Phys. J. B* **89**, 2 (2016).
- [60] R. Zhu, J.-H. Dai, and Y. Guo, *J. Appl. Phys.* **117**, 164306 (2015).
- [61] R. Zhu, C. Cai, *J. Appl. Phys.* **122**, 124302 (2017).
- [62] S. Bera and I. Mandal 2021 *J. Phys.: Condens. Matter*

33 295502.

- [63] S. Bera, S. Sekh, I. Mandal, Ann. Phys. (Berlin) **535**, 2200460 (2023).
- [64] A. Gregefalk, A. Black-Schaffer, T. Nag, arXiv:2306.08759 (2023).
- [65] W. Li and L. E. Reichl, Phys. Rev. B **60**, 15732 (1999).
- [66] Y. M. Blanter and M. Büttiker, Physics reports **336**, 1 (2000).
- [67] M. Milicevic, G. Montambaux, T. Ozawa, O. Jamadi, B. Real, I. Sagnes, A. Lemaitre, L. Le Gratiet, A. Harouri, J. Bloch, and A. Amo, Phys. Rev. X **9**, 031010 (2019).
- [68] A. Cortijo, D. Kharzeev, K. Landsteiner, M. A. H. Vozmediano, Phys. Rev. B **94**, 241405(R) (2016).
- [69] D. I. Pikulin, Anffany Chen, and M.Franz, Phys. Rev. X **6**, 041021 (2016).
- [70] A. G. Grushin, J. W. F. Venderbos, A. Vishwanath, and R. Ilan, Phys. Rev. X **6**, 041046 (2016).
- [71] R. W. Bomantara and J. Gong, Phys. Rev. B **94**, 235447 (2016).
- [72] [M. O. Goerbig, J.-N. Fuchs, G. Montambaux, and F. Piechon, Phys. Rev. B **78**, 45415 (2008).
- [73] H-Y Lu, A. S. Cuamba, S-Y Lin, L. Hao, R. Wang, H. Li, Y. Zhao, and C. S. Ting, Phys. Rev. B **94**, 195423 (2016).
- [74] A. D. Zabolotskiy and Yu. E. Lozovik, Phys. Rev. B **94**, 165403 (2016).
- [75] R. G. Polozkov, N. Y. Senkevich, S. Morina, P. Kuzhir, M. E. Portnoi, and I. A. Shelykh, Phys. Rev. B **100**, 235401 (2019).
- [76] J-P. Lang, H. Hanafi, J. Imbrock, and C. Denz, Phys. Rev. A **107**, 023509 (2023).